Journal of Catalysis 271 (2010) 178–185

Contents lists available at ScienceDirect

Journal of Catalysis

journal homepage: www.elsevier.com/locate/jcat

Glycine–nitrate combustion synthesis of CuO–ZnO–ZrO_2 catalysts for methanol synthesis from CO_2 hydrogenation

Xiaoming Guo [a,b], Dongsen Mao [b,*], Guanzhong Lu [a,b,*], Song Wang [b], Guisheng Wu [b]

[a] Research Institute of Industrial Catalysis, East China University of Science and Technology, Shanghai 200237, PR China
[b] Research Institute of Applied Catalysis, School of Chemical and Environmental Engineering, Shanghai Institute of Technology, Shanghai 200235, PR China

ARTICLE INFO

Article history:
Received 21 October 2009
Revised 6 January 2010
Accepted 7 January 2010
Available online 1 February 2010

Keywords:
CuO–ZnO–ZrO_2 catalyst
Glycine–nitrate combustion synthesis
CO_2 hydrogenation
Methanol

ABSTRACT

A series of CuO–ZnO–ZrO_2 (CZZ) catalysts were synthesized by a glycine–nitrate combustion method and characterized by XRD, BET, N_2O chemisorption, SEM and TPR techniques. The results show that the physicochemical properties of the catalysts are strongly influenced by the fuel content used in the combustion process. The dispersion of CuO exhibits an inverse-volcano variation trend with an increase in the glycine amount from 50% to 150% of the stoichiometry. The relationship between physiochemical properties and the fuel content is discussed in detail in terms of combustion temperature. The catalytic performance for the synthesis of methanol from CO_2 hydrogenation was examined. The CZZ catalyst exhibits an optimum catalytic activity when 50% of stoichiometric amount of glycine was used. The turnover frequency has been calculated for various CZZ catalysts, and it reveals that the catalytic activities depend not only on the surface area of metallic copper but also on the phase state of ZrO_2.

1. Introduction

It is well known that carbon dioxide is the most important greenhouse gas. With the increase in carbon dioxide concentration in the atmosphere, global warming problems are becoming more and more serious in recent years. Conversion of carbon dioxide to useful chemicals and fuels is one of the most promising ways to mitigate the problem. Most of the existing research focuses on methanol synthesis from CO_2 because methanol is a common chemical feedstock for several important chemicals and a potential alternative energy to fossil fuels [1,2].

CuO–ZnO–Al_2O_3 catalysts have been widely used for methanol synthesis from syngas ($CO + H_2$); however, they exhibited a poor catalytic performance for the hydrogenation of CO_2 [3,4]. The reason can be ascribed to the negative effect of water on the rate of methanol formation and the strong hydrophilic characteristic of alumina [3]. Zirconia-supported copper catalysts, which show an interesting catalytic behavior for CO_2 hydrogenation, have been well documented [3–14]. Among them, CuO–ZnO–ZrO_2 (CZZ) or modified-CZZ has gained an increasing interest for its high activity in recent years [3,4,8–14]. Apart from catalyst compositions, preparation methods have a considerable influence on the catalytic performance [3,15,16]. Numerous methods such as co-precipitation [7–10,14], impregnation [17] and sol–gel [5,18] have been developed to prepare copper-based oxide catalysts. However, these methods are pH sensitive, time consuming or restricted by the deviation from stoichiometry and the requirement of expensive precursors [15,19,20]. Compared with those traditional methods, the combustion synthesis method, based on the principles of the propellant chemistry, has many advantages such as precise stoichiometric ratio, homogeneous component, low cost and short reaction time. Therefore, it has been an attractive technique for the synthesis of metal oxide powders in recent years [13,21–26]. In the combustion synthesis process, a thermally induced redox reaction takes place between an oxidant and a fuel. In general, the metal nitrates acting as cation sources are used as oxidants, whereas organic compounds such as citric acid, urea and glycine are employed as fuels [27–29]. The combustion characteristics are closely related to the selection of fuel. A good fuel should react non-violently and act as a complexant for metal cations [27]. Glycine, one of the simple amino acids, is known to act as a complexing agent for a number of metal ions since it has a carboxylic acid group at one end and amino group at the other end. Such types of zwitterionic character of a glycine molecule can effectively complex metal ions of varying ionic sizes, which helps in preventing their selective precipitation and maintaining compositional homogeneity among the constituents [27,28]. Therefore, glycine-nitrate combustion synthesis has been a very popular combustion method for the preparation of metal oxide powders [22,27,28]. Arena et al. [13] prepared CZZ catalyst

* Corresponding authors. Address: Research Institute of Applied Catalysis, School of Chemical and Environmental Engineering, Shanghai Institute of Technology, Shanghai 200235, PR China. Fax: +86 21 6494 1386.
E-mail addresses: dsmao1106@yahoo.com.cn (D. Mao), gzhlu@ecust.edu.cn (G. Lu).

0021-9517/$ - see front matter © 2010 Elsevier Inc. All rights reserved.
doi:10.1016/j.jcat.2010.01.009

with a combustion method and investigated its catalytic action for methanol synthesis via CO_2 hydrogenation. However, the fuel of oxalic-di-hydrazide employed in their work is toxic (carcinogenic), and no related discussion about the combustion reaction was reported.

In this paper, we report the synthesis of CZZ catalysts using the glycine-nitrate combustion method and examine their catalytic properties for methanol synthesis from CO_2 hydrogenation. The combustion reactions are analyzed in terms of propellant chemistry, and the combustion behaviors are described as well. The prepared CZZ catalysts have been characterized by XRD, BET, SEM, H_2-TPR and reactive N_2O adsorption techniques. Since fuel content is an important parameter in combustion synthesis, the effect of different glycine amounts on the properties of the derived CZZ catalysts is discussed in detail. Furthermore, the catalytic performances of the CZZ catalysts are discussed in relation to the results of physicochemical characterization.

2. Experimental

2.1. Catalyst preparation

First, analytical-grade $Cu(NO_3)_2{\cdot}3H_2O$, $Zn(NO_3)_2{\cdot}6H_2O$ and $Zr(NO_3)_4{\cdot}5H_2O$ were dissolved in deionized water to form a transparent solution in which Cu^{2+}, Zn^{2+} and Zr^{4+} concentrations meet the formula of $(CuO)_{0.5}(ZnO)_{0.2}(ZrO_2)_{0.3}$ (CZZ). Then, the glycine solution was slowly added to the metal nitrate aqueous solution under constant stirring. The resulting mixture was kept in an ultrasound bath operating at 47 kHz with a power of 30 W until a blue and transparent sol was obtained. Afterwards, the crucible was transferred to an open muffle furnace preheated at 493 K. With the evaporation of water, the sol converted to a viscous gel and then the gel ignited spontaneously with rapid evolution of a large quantity of gases, yielding a foamy, voluminous powder. Because the time for the autoignition is rather short, to remove traces of undecomposed glycine, nitrates and their decomposition products, the powder was further heated at 723 K for 3 h. To investigate the effect of different glycine amounts on CZZ characteristics, glycine addition was set from 50% to 150% of the stoichiometric amount which can be calculated according to propellant chemistry. The obtained CZZ powder was termed as 50-CZZ, 75-CZZ, 100-CZZ, 125-CZZ and 150-CZZ.

2.2. Catalyst characterization

The dried semisolid gel obtained by heating the sol at 383 K for 8 h was collected prior to combustion reaction for a thermal analysis measurement. The thermal gravimetric and differential thermal analysis (TG–DTA) profiles were recorded on a thermal analyzer (SDT Q-600, Thermal Analysis Instruments) at a heating rate of 10 K/min under a continuous-flow of air. X-ray diffraction (XRD) analysis of a sample was performed using a PANalytical X'Pert diffractometer operating with Ni β-filtered Cu Kα radiation at 40 kV and 40 mA. Two theta angles ranged from 10° to 70° with a speed of 6° per minute. The crystallite size was then calculated from the XRD spectra by using the Scherrer equation. Full nitrogen adsorption/desorption isotherms at 77 K were obtained after outgassing the sample under vacuum at 473 K for 3 h, using a Micromeritics ASAP2020 M+C adsorption apparatus. Specific surface area (S_{BET}) was calculated using a value of 0.162 nm^2 for the cross-sectional area of the nitrogen molecule. The surface morphology was observed by the scanning electronic microscopy (SEM, S-3400 N, Hitachi). The metallic copper surface area (S_{Cu}) in the reduced catalyst was determined using a N_2O chemisorption method similar to that described by Chinchen et al. [30]. The measurements were carried out in a linear quartz microreactor. The catalyst (0.2 g) was reduced in an H_2/He mixture at 523 K for 1 h. Then, it was purged with He and cooled to the chemisorption temperature (333 K). A flow of 1 vol% N_2O/He gas mixture was fed into the reactor. The N_2 produced by the decomposition of N_2O on the exposed Cu atoms was detected using a mass spectrometer (Pfeiffer Vacuum Quadstar, 32-bit). The copper surface area was calculated assuming an atomic copper surface density of 1.46×10^{19} Cu atoms/m^2 and a molar stoichiometry of N_2O/Cu = 0.5 [11]. Temperature-programmed reduction (TPR) was carried out by using 10 vol% H_2/N_2 as a reducing gas in a linear quartz microreactor. Approximately 30 mg of a freshly calcined catalyst was placed on top of glass wool in the reactor. The outlet of the reactor was connected to a glass column packed with molecular sieve 5 Å in order to remove the moisture produced from reduction. The flow rate of the reducing gas was kept at 30 ml/min, and the temperature was raised from 373 to 573 K at a rate of 5 K/min. The amount of consumed H_2 was measured by a thermal conductivity detector (TCD).

2.3. Catalyst testing

Activity and selectivity measurements for CO_2 hydrogenation were carried out in a continuous-flow, fixed-bed reactor. About 0.5 g of catalyst diluted with quartz sand (both in 20–40 mesh) was packed into the stainless steel tubular reactor. Prior to the catalytic measurements, the fresh catalyst was reduced in a stream of 10 vol% H_2/N_2 at 573 K for 3 h under atmospheric pressure. Then, the reactor was cooled to 433 K and the reactant gas (CO_2:H_2 = 1:3, molar) flow was introduced, raising the pressure to 3.0 MPa and the temperature to a given temperature. The flow rate of reactant gas was controlled by a mass flow controller (5850E, Brooks). The total pressure was regulated with a back pressure regulator (Go Co.) placed on the exit of the reactor. The reaction temperature was controlled by a temperature controller and measured with a chromel–alumel thermocouple. All post-reactor lines and valves were heated to 413 K to prevent product condensation. Effluent products were analyzed on-line with a gas chromatograph (6820, Agilent). Methanol was determined with a Porapak Q column, a FID detector and Carbosieve column, TCD detector for other gaseous product were used. Conversion and selectivity values were calculated by mass balance methods, and the steady-state values are quoted as the average of four different analyses taken after 4 h on stream operation.

3. Results and discussion

3.1. Combustion reaction analysis and combustion behavior

For glycine-nitrate combustion, primarily N_2, CO_2 and H_2O are evolved as the gaseous products [28,31]. Thus, the combustion reaction in the present paper can be represented as follows:

$$\begin{aligned} &1/2Cu(NO_3)_2\cdot 3H_2O + 1/5Zn(NO_3)_2\cdot 6H_2O + 3/10Zr(NO_3)_4\cdot 5H_2O \\ &\quad + mH_2NCH_2COOH + (9m/4 - 13/4)O_2 \\ &\rightarrow (CuO)_{0.5}(ZnO)_{0.2}(ZrO_2)_{0.3} + (m/2 + 13/10)N_2 \\ &\quad + (5/2m + 21/5)H_2O + 2mCO_2 \end{aligned} \quad (1)$$

According to the principle of propellant chemistry [32], for stoichiometric redox reaction between a fuel and an oxidizer, the ratio of the net oxidizing valence of the metal nitrate to the net reducing valence of the fuel should be unity. In this case, 1 mol CZZ stoichiometrically requires 13/9 mol glycine (i.e. m = 13/9) without the necessity of getting oxygen from outside. When the glycine amount is smaller than that of stoichiometry, the combustion reaction is called a fuel-deficient reaction. The value of $(9m/4 - 13/4)$

would be negative suggesting that O_2 would be evolved in the products. However, when the glycine amount is larger than stoichiometric, corresponding to fuel-rich condition, atmospheric O_2 would be involved to ensure the complete combustion of glycine [27].

The glycine amount will affect the value of combustion enthalpy, which can be expressed as:

$$\Delta H^0 = \left(\sum n\Delta H_f^0\right)_{\text{products}} - \left(\sum n\Delta H_f^0\right)_{\text{reactants}} \quad (2)$$

where n is the number of the mole and ΔH_f^0 is the formation enthalpy of the reactants or products. Using the thermodynamic data of various reactants and products available in the literature [33], the enthalpy of combustion can be calculated. The variation of enthalpy with the glycine amount can be seen in Table 1. As expected, the enthalpy increases substantially with the amount of glycine used in the combustion reaction. Accompanied with the heat release, large amounts of gases are evolved during the combustion process. Table 1 shows that the number of mol of the gases evolved also increases as the glycine amount increases, and it ranges from 9.1 mol for 50-CZZ to 16.3 mol for 150-CZZ.

Different combustion phenomena resulting from different amounts of glycine used in the mixtures have been observed. As shown in Table 1, 50-CZZ exhibits a smoldering combustion type, whereas the other samples show incandescent flame growing after autoignition. The maximum combustion intensity is observed at the stoichiometric glycine amount. In addition to that, the duration of combustion also changes with the variation of glycine amount and a minimum being only 2–4 s (sample 100-CZZ), as shown in Table 1.

The combustion behavior of the dried gel collected prior to decomposition was recorded by TG and DTA. A typical TG–DTA plot for the sample of 100-CZZ is shown in Fig. 1. It can be seen that in the temperature range of 323–450 K, a weight loss of about 5% occurs, which is attributed to the vaporization of physically absorbed water and the dehydration reaction of gels. The appearance of an abrupt and large weight loss in a very narrow temperature range (450–493 K) with a sharp exothermic peak around 464 K clearly indicates the vigorous combustion reaction between glycine and NO^{3-}. Corresponding to a wide temperature region from 493 to 723 K, there is a slight weight loss and one broad and small exothermic region, which can be ascribed to the burning of the residual glycine entrapped in the powder [34]. The total weight loss determined for the production of 100-CZZ was 80.5%, and it was approximate to the theoretical value of 77.7%. These results of thermoanalysis give a strong evidence for the adoption of 493 K as the initiation temperature to initiate the combustion reaction and 723 K as the calcination temperature to ensure complete decomposition of catalyst precursor and to minimize the sintering of CZZ powders as well.

3.2. Textural and structural properties

Fig. 2 shows the XRD patterns of CZZ catalysts prepared with different amounts of glycine. The diffraction lines of CuO (JCPDS 80-1268) were observed at 2θ of 35.6°, 38.8° and 48.9°. With the increase in the glycine amount from 50% to 100% of stoichiometry, the diffraction lines of CuO become stronger and sharper, indicating a continuous increase in the crystallization degree of CuO. The crystallite size of CuO, which is estimated using the Scherrer equation, increased from 16 nm of 50-CZZ to 25.3 nm of 100-CZZ, as shown in Table 2. However, the XRD patterns of 125-CZZ and 150-CZZ show that further increase in glycine amount results in a small decrease in diffraction line intensity, which represents a slight decrease in crystallite size of CuO. Furthermore, it can be seen from Fig. 2 that the diffraction lines of ZnO phase (JCPDS 36-1451) appear at 2θ of 34.5° and 36.3°. The variation trend of ZnO phase with the change of glycine amount is similar to that of CuO phase.

It is noteworthy that the amount of glycine has remarkable effect on the formation of zirconia phase. For 50-CZZ, the diffraction lines of both tetragonal zirconia (t-ZrO_2, 2θ = 30.3°) and monoclinic

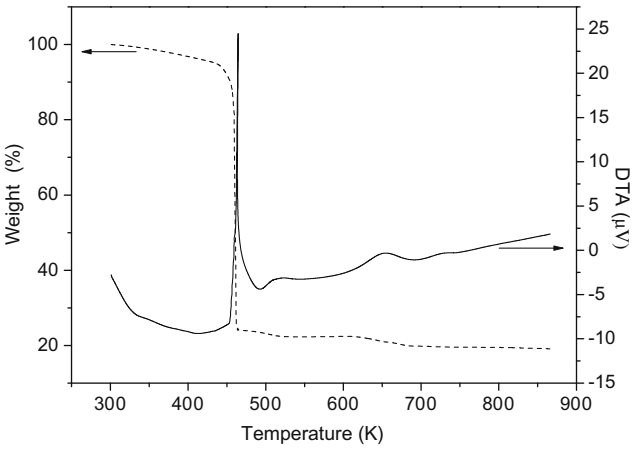

Fig. 1. TG and DTA profiles for the dried gel of 100-CZZ sample.

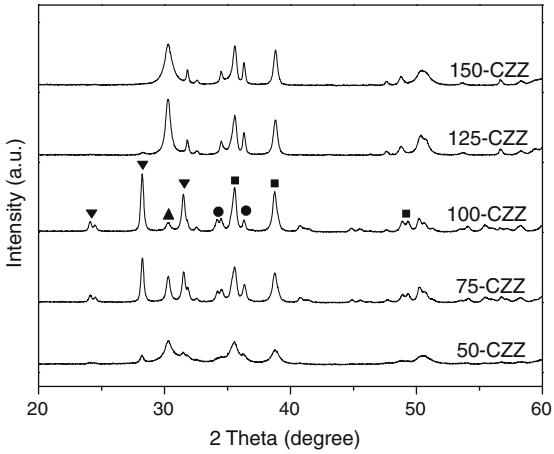

Fig. 2. XRD patterns of CuO–ZnO–ZrO_2 catalysts prepared with different amounts of glycine. (■) CuO; (●) ZnO; (▲) ZrO_2 (tetragonal); (▼) ZrO_2 (monoclinic).

Table 1
Characteristics of the combustion reaction with different amounts of glycine.

Catalysts	Moles of glycine, 1 mol CZZ	ΔH^0 (kJ/mol)	Moles of gas, 1 mol CZZ	Duration time of combustion (s)	Combustion type
50-CZZ	0.72	−147	9.1	50–60	Smolder
75-CZZ	1.08	−458	10.9	5–8	Flame
100-CZZ	1.44	−770	12.7	2–4	Flame
125-CZZ	1.81	−1081	14.5	25–30	Flame
150-CZZ	2.17	−1393	16.3	35–40	Flame

Table 2
Physicochemical properties of the CuO–ZnO–ZrO_2 catalysts prepared with different amounts of glycine.

Catalysts	CuO crystallite size (nm)	$n(m\text{-}ZrO_2)/n(t\text{-}ZrO_2)$[a]	S_{BET} (m^2/g)	S_{Cu} (m^2/g)
50-CZZ	16.0	0.85	17.8	3.32
75-CZZ	19.7	3.30	4.8	1.20
100-CZZ	25.3	10.30	3.3	0.75
125-CZZ	23.0	0.49	4.8	1.26
150-CZZ	19.5	0.07	5.5	1.50

[a] The molar ratio of m-ZrO_2 to t-ZrO_2 estimated using semiquantitative method with X'Pert Highscore software and ICDD2.

ZrO_2 (m-ZrO_2, $2\theta = 24.1°, 28.2°, 31.5°$) are weak and broad, demonstrating that the zirconia exhibits amorphous or semicrystalline nature in a certain extent. When the glycine amount rises to 75% of stoichiometry, the intensities of the diffraction lines increase drastically accompanied with an obvious increase in the ratio of m-ZrO_2 to t-ZrO_2. A maximum in the intensity of the diffraction line from m-ZrO_2 is obtained as the glycine amount reached 100% of stoichiometry. At the same time, the ratio of m-ZrO_2 to t-ZrO_2 reaches a maximum, as shown in Table 2. In contrast to the 100-CZZ, a significant increase in the intensities of t-ZrO_2 diffraction lines can be observed for 125-CZZ and 150-CZZ at the expense of m-ZrO_2 diffraction lines. These results confirmed that a phase transformation between tetragonal and monoclinic occurred with the change of glycine amount used in the combustion reaction.

The BET surface areas derived from nitrogen physisorption are listed in Table 2. An increase in the glycine amount leads to a marked decrease in the BET surface area. The minimum surface area was obtained for 100-CZZ prepared with the stoichiometric glycine amount, and then a slight increase in surface area appeared for 125-CZZ and 150-CZZ. This result is in accordance with the results regarding crystallite size, as determined from XRD. The specific surface areas of the catalysts are quite low and the maximum is 17.8 m^2/g for 50-CZZ. In related work, Arena et al. [13] reported that the BET surface areas of CZZ samples with the Cu/Zn atomic ratio in the rang of 0.2–3.0 ranged from 10 to 24 m^2/g. Similar surface area values also have been reported by Schuyten et al. for PdO–CuO–ZnO–ZrO_2 catalysts [35]. Moreover, the metallic copper surface area was measured by reactive N_2O adsorption technique. As shown in Table 2, the variation trend of metallic copper surface area with glycine amount is similar to that of BET surface area. The maximum of 3.32 m^2/g is obtained over the sample 50-CZZ and the minimum of 0.75 m^2/g is obtained over 100-CZZ. Similar values of metallic copper surface area (1.9–5.7 m^2/g) were found earlier by Arena et al. [13]. Because the value of metallic copper surface area is a mirror of the dispersion of CuO, 50-CZZ and 100-CZZ possess the highest and the lowest dispersion of CuO, respectively.

The SEM pictures of CZZ powders show a clear change in morphology as the fuel content used in the combustion increases from 50% to 150% of stoichiometry. As shown in Fig. 3a, the 50-CZZ exhibits a cotton-like morphology and no aggregation of particle can be found. When stoichiometric amount of glycine was used, an irregularly shaped agglomerates with a few pores were observed, indicating a large particle size and a small surface area for 100-CZZ. The sample 150-CZZ shows honeycomb morphology, and it is more porous and looser than 100-CZZ since more gases released in the combustion process.

For combustion synthesis, the structure and texture of products are mainly determined by the combustion temperature. It is well known that products with large particle size, small BET surface and high degree of sintering are obtained at a high combustion temperature. Since the combustion is not an adiabatic process, for a given combustion reaction, the combustion temperature is related to the following factors:

- The combustion enthalpy: with the increase in fuel amount, the combustion heat released by the combustion reaction increases and a lager combustion heat will result in a higher combustion temperature.
- The duration of combustion: conditioning on that the combustion enthalpy keeps constant, the shorter the duration of combustion is, the higher the combustion temperature will be [36]. The reason for this is that the heat dissipated in a short time is small and most of the combustion heat is imposed on heating the products. The duration of combustion is mainly affected by the fuel content; the closer it is to the stoichiometry value, the shorter the duration will be.
- The amount of the gases evolved: the gaseous products evolved during the combustion dissipate the heat of combustion and impede the rise of temperature. The amount of the gases evolved changes with the variation of fuel content. Furthermore, the gas evolution also helps in limiting the interparticle contact and hinders particle growth [28].

Apparently, the combustion temperature is determined by competitive results of these factors. At the same time, it can be seen that all these factors are connected with the fuel content. However, no agreement exists in the literature with respect to the effect of the fuel content on the structure and texture of products. For instance, different variation trends of particle size with fuel content were reported in literature. Some authors found that with the increase in fuel content, the particle size of products increase [22,37], whereas opposite trend had been observed by Zhang and Gao [38]. Most studies reported that a volcano trend of the particle size occurred with the change of fuel content [27,39]. The disagreement of these reports is due to the different fuel and metal cations involved in different laboratory. Similar viewpoint had been proposed by Deganello et al. [37].

In our case, the reaction of preparing 50-CZZ exhibits a smoldering combustion type since a small combustion heat is released. The maximum combustion intensity is observed with the fuel content of stoichiometric, which indicates that the combustion temperature is the highest. The reasons are ascribed to the large combustion enthalpy and the short duration of combustion, as shown in Table 1. For the fuel-rich reaction, the amount of the gases evolved is large and the duration of combustion is long, although the combustion enthalpy is large too. The two former factors are predominant, thereby the combustion intensity for 125-CZZ and 150-CZZ is weaker than that for 100-CZZ. Based on these analyses, it is easy to understand that the crystallite size of CuO and the extent of agglomeration increase firstly and then decrease (i.e. a volcano trend) from 50-CZZ to 150-CZZ, accompanied with an inverse-volcano trend of BET surface area. The phenomena of ZrO_2 phase transformation also can be explained in terms of combustion temperature, since transformation from t-ZrO_2 to m-ZrO_2 occurs with the rise of temperature [40].

3.3. The reducibility of catalyst

In order to investigate the reduction behavior of the CCZ catalysts, TPR measurements were carried out. As shown in Fig. 4,

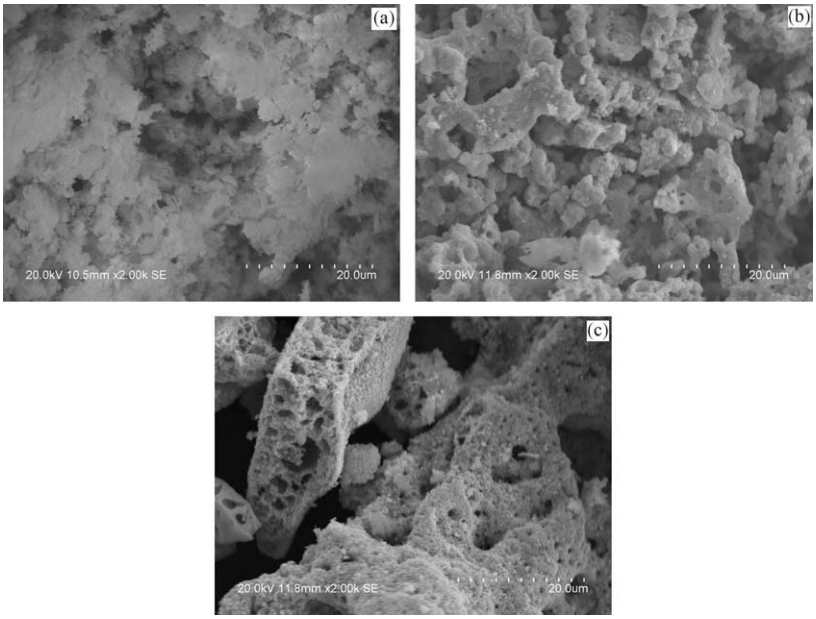

Fig. 3. SEM micrographs of CuO–ZnO–ZrO_2 catalysts: (a) 50-CZZ; (b) 100-CZZ; (c) 150-CZZ.

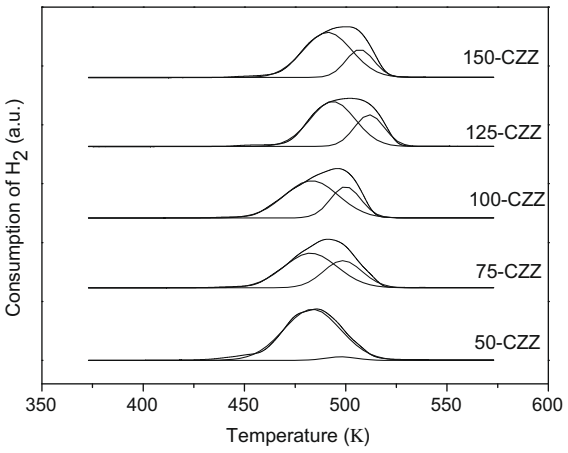

Fig. 4. H_2–TPR profiles of the CuO–ZnO–ZrO_2 catalysts.

the reduction profiles of all the samples prepared with different glycine amount exhibit a broad band of H_2 consumption in the range of 440–540 K. To gain more insight into the TPR results, the broad band of H_2 consumption are deconvoluted into two peaks, which are denoted as α and β peak. The peak positions and their contributions are summarized in Table 3. Since ZnO and ZrO_2 are not reduced within the experimental region [24,41,42], the two peaks are ascribed to the reduction of two different types of CuO phase. Obviously, copper oxide species in the CZZ catalysts are reduced at much lower temperatures when compared to pure CuO, which is reported to be reduced at *ca.* 570 K [3]. These results indicate that ZrO_2 and ZnO can promote the dispersion of copper oxide and enhance the reducibility of the copper phase, a fact that is consistent with previous observations [24,40–43].

The low temperature peak (α peak) is attributed to the reduction of highly dispersed CuO strongly interacting with ZrO_2 and ZnO, whereas the peak appearing at higher temperature (β peak) is due to the reduction of bulk CuO [26,41]. As shown in Table 3, the relative contribution of α peak to the TPR pattern decreases as the glycine amount increases and a minimum of 68.0% is found for 100-CZZ. A gradual increase appears when the glycine amount exceeds 100% of the stoichiometry. The result indicates that the amount of easily reducible well-dispersed copper oxide, from 50-CZZ to 150-CZZ, takes on an inverse-volcano variation trend and it is in good agreement with the results of XRD and S_{Cu}. As to the reduction temperature, many researchers believe that the smaller the CuO particles is, the lower the reduction temperature should be [20,26,41]. However, Rhodes and Bell found that the reducibility of supported CuO depended not only on the particle size but also on the phase state of ZrO_2 [43]. They reported that even though the dispersion of CuO on *t*-ZrO_2 is higher than that on *m*-ZrO_2, it is reduced at a significantly higher temperature. As mentioned above in the XRD patterns, a phase transformation from *m*-ZrO_2 to *t*-ZrO_2 occurs when the glycine amount exceeds 100% of stoichiometry. As a consequence, the position of α peak (494 and 491 K) for 125-CZZ and 150-CZZ is higher than that of 100-CZZ (483.1 K), although the dispersion of CuO on 125-CZZ and 150-CZZ is higher than that on 100-CZZ.

Table 3
Temperature of reduction peaks and their contributions to the TPR pattern over CuO–ZnO–ZrO_2 catalysts prepared with different amounts of glycine.

Catalysts	T_α (K)	T_β (K)	$A_\alpha/(A_\alpha + A_\beta)$[a] (%)
50-CZZ	484	498	96.5
75-CZZ	483	499	69.5
100-CZZ	483	500	68.0
125-CZZ	494	512	70.1
150-CZZ	491	507	76.0

[a] A_α and A_β represent the area of α and β peak, respectively.

3.4. Catalytic performance

The catalytic activity and selectivity of methanol on various catalysts are presented in Table 4. CO and methanol are the only carbon-containing products under the reaction conditions, and traces of methane can be detected at high temperatures. As illustrated in Table 4, the conversion of CO_2 declined with the elevation of glycine amount until it reached a minimum of 3.5% for 100-CZZ. Then, an increase appears again for 125-CZZ and 150-CZZ. As well

Table 4
Catalytic performance for the hydrogenation of CO_2 to methanol over CuO–ZnO–ZrO_2 prepared with different amounts of glycine.

Catalysts	CO_2 conversion (%)	CH_3OH selectivity (%)	CH_3OH yield (%)	TOF of $CH_3OH \times 10^3$ (s^{-1})
50-CZZ	12.0	71.1	8.5	11.8
75-CZZ	4.9	80.0	3.9	15.0
100-CZZ	3.5	82.1	2.9	17.8
125-CZZ	5.0	79.1	4.0	14.6
150-CZZ	5.9	78.9	4.7	14.4

Reaction conditions: $H_2/CO_2 = 3$, $T = 493$ K, $P = 3.0$ MPa, GHSV = 3600 h^{-1}.

known, for copper-based catalysts, finely dispersed CuO species are responsible for catalytic activity [26,40]. Therefore, the variation trend of catalytic activity is easy to understand by considering the similar trend of the dispersion of CuO, which had been demonstrated by XRD and TPR measurements. Furthermore, it is noteworthy that the CH_3OH selectivity is also affected by the glycine amount. A volcanic shape of the methanol selectivity versus glycine amount is observed, and the 100-CZZ exhibits the maximum of 82.1%. It can be ascribed to the volcano variation trend of the ratio of *m*-ZrO_2 to *t*-ZrO_2 with the glycine amount, as shown in Fig. 5. The methanol selectivity over *m*-ZrO_2-supported catalysts is higher than that over *t*-ZrO_2-supported catalysts, and similar results for CO hydrogenation had been reported by Rhodes and Bell [43]. Since the variation of the CH_3OH selectivity is much less than that of CO_2 conversion, the sequence of methanol yield on various catalysts is determined mainly by the latter. As seen in Table 4, the maximum methanol yield of 8.5% was obtained over the 50-CZZ catalyst. Under the same reaction conditions, the value of methanol yield is 6.9% over the CZZ catalyst with the same composition but prepared by conventional carbonate co-precipitation method [44].

The metallic copper surface area (S_{Cu}) determined by means of N_2O chemisorption is an important parameter for Cu-based catalysts since it is related closely to the catalytic activity of catalysts. Turnover frequency (TOF) of methanol formation, which represents the molecular number of methanol formed per second per metallic copper atom, had been calculated from the S_{Cu} for various catalysts, and the results are listed in Table 4. It can be seen that the values of TOF varied in the range of $11.8–17.8 \times 10^{-3}$ s^{-1}, and approximate values ($0.5–10.5 \times 10^{-3}$ s^{-1}) under 0.9 MPa and 493 K were reported by Arena et al. [13]. Fig. 6a shows the relationship between TOF and Cu particle size (d_{Cu}) which was calculated from the surface area of metallic copper using a spherical particle model [45]. Obviously, with the decrease in d_{Cu}, the value of TOF decreases. The same variation trend can be found in the literature [3,12]. These results indicate the structurally sensitive character of the title reaction. To better understand the role of metallic copper in the process of hydrogenation of CO_2, TOF is also plotted versus S_{Cu}. As shown in Fig. 6b, the TOF of methanol formation decreases as the metallic copper surface area increases. The result reveals that the activity of a catalyst is not only related to S_{Cu} but also to other causes, because the plot of TOF versus S_{Cu} should be a horizontal line if the S_{Cu} is the sole cause affecting the catalytic activity of the catalyst [45,46]. Other causes affecting the catalytic activity of the catalyst have been proposed by different groups. It is a popular viewpoint that "multisite" including Cu^0 and Cu^+ centers are involved in and the stabilization of the Cu^+ ions favors the hydrogenation of CO_2 [47–50]. Some authors reported that the activity

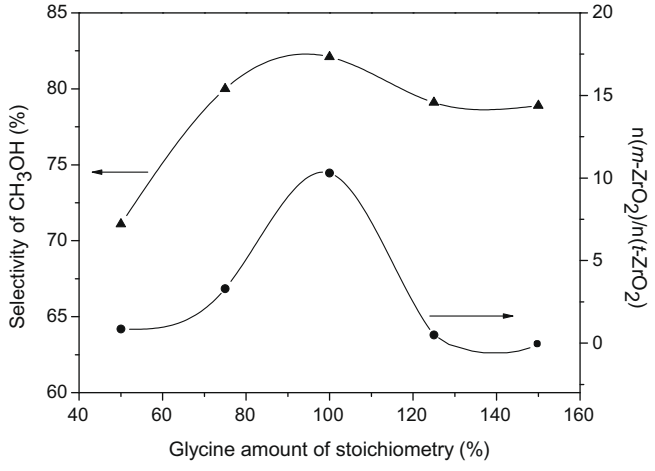

Fig. 5. Effect of the amount of glycine on the selectivity of methanol and the molar ratio of *m*-ZrO_2 to *t*-ZrO_2 over CuO–ZnO–ZrO_2 catalysts. Reaction conditions: $H_2/CO_2 = 3$, $T_R = 493$ K, $P = 3.0$ MPa, GHSV = 3600 h^{-1}.

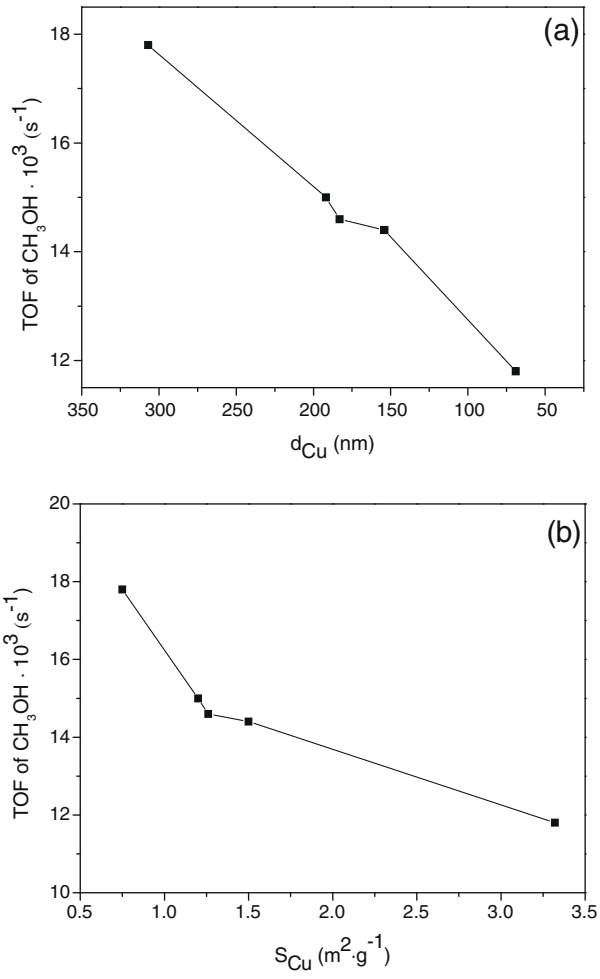

Fig. 6. The relationship between the TOF of methanol formation and the Cu particle size (a) and Cu specific surface area (b). Reaction conditions: $H_2/CO_2 = 3$, $T_R = 493$ K, $P = 3.0$ MPa, GHSV = 3600 h^{-1}.

of Cu sites is different when it locates at different positions of the crystal structure [48,51,52]. Furthermore, a lot of studies believe that there is a synergy between the metal and the oxide components, which is considered to contribute to the catalytic activity of the catalyst [8,40,45]. In our experiment, with the increase in the relative amount of m-ZrO_2 (i.e. $n(m\text{-}ZrO_2)/[n(t\text{-}ZrO_2) + n(m\text{-}ZrO_2)]$) for different CZZ samples, TOF increased and a linear relation between them was found, as shown in Fig. 7. This indicates that the phase state of ZrO_2 is an important factor affecting the catalytic activity of the CZZ catalysts. The conclusion is consistent with the results of Jung and Bell [53]. They reported that the methanol synthesis activity over m-ZrO_2 was significantly higher than that over t-ZrO_2 under the condition of identical ZrO_2 surface area and Cu dispersion, which they argued to be due to the higher concentration of intermediates to methanol over m-ZrO_2. It should be noted, though, that the TOF of 50-CZZ (the relative amount of m-ZrO_2 is 45.9%) deviated from the linear relation severely. This can be explained by taking into account the following causes:

- The studies of mechanism of methanol synthesis show that the rate-limiting step is the formation and hydrogenation of the reactive intermediates such as formate and methoxide [11,54], which depends on the concentration of H atoms on the surface of ZrO_2. Rhodes and Bell reported that when the surface area of Cu was greater than 2.5 m^2/g, the surface of ZrO_2 was saturated with H atoms provided by spillover from Cu [54]. Further increase in the surface of metallic Cu is invalid for the methanol synthesis, and this leads to a lower TOF. As shown in Table 2, the surface area of Cu is 3.32 m^2/g for 50-CZZ, thereby, a lower TOF was obtained over it.
- Compared with the other samples, the combustion temperature for 50-CZZ during the process of combustion synthesis is lower and all the components appear mainly in an amorphous or semicrystalline phase, which had been demonstrated in the XRD pattern. Thus, a weaker synergy exists between the metal and the oxide components, resulting in a lower TOF for 50-CZZ.

The effects of reaction temperature on the catalytic performances of CZZ catalysts are presented in Fig. 8. It can be seen that the conversion of CO_2 increases but the CH_3OH selectivity decreases along with the elevation of reaction temperature. The results are consistent with the reports in the literature [3,41,42]. As well known, the synthesis of methanol and the reverse water–gas shift (RWGS) are the two parallel reactions involved in the CO_2 hydrogenation process. The equilibriums can be described as:

$$CO_2 + 3H_2 \leftrightharpoons CH_3OH + H_2O \quad \Delta H_{298} = -49.47\ \text{kJ/mol} \tag{3}$$

$$CO_2 + H_2 \leftrightharpoons CO + H_2O \quad \Delta H_{298} = 41.17\ \text{kJ/mol} \tag{4}$$

Obviously, raising temperature is favorable for the reaction of RWGS because of its endothermic character. Meanwhile, compared to methanol synthesis, the RWGS reaction has a higher apparent activation energy [42,48], which means that the increase in CO production is faster than that of methanol with increase in temperature. Consequently, in the whole temperature range, the CH_3OH selectivity decreases along with the elevation of reaction temperature. The variation of methanol yield with reaction temperature is shown in Fig. 9, and it can be explained as follows. On one hand, as shown in reaction (3), the synthesis of methanol is an exothermic reversible reaction and its equilibrium constant decreases with an increase in the temperature. On the other hand, the rate of reaction increases kinetically with the increase in temperature. Therefore, the product distribution will be controlled by both thermodynamics and kinetics. A maximum yield of methanol which represents the critical point of the reaction transforming from kinetics to thermodynamics exists [45], as shown in Fig. 9. According to the linear

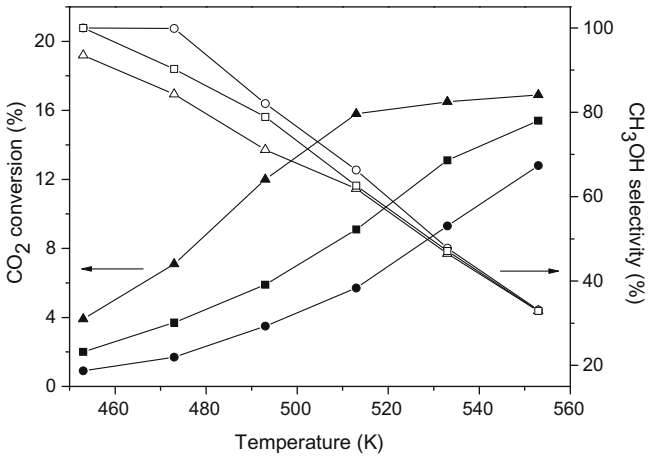

Fig. 8. Effect of temperature on the conversion of CO_2 (solid symbols) and selectivity of methanol (open symbols) over CuO–ZnO–ZrO_2 catalysts: (triangles) 50-CZZ; (circles) 100-CZZ; (rectangles) 150-CZZ. Reaction conditions: $H_2/CO_2 = 3$, $P = 3.0$ MPa, GHSV = 3600 h^{-1}.

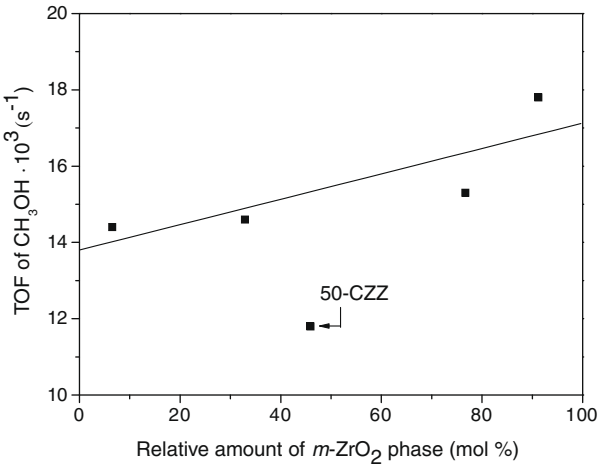

Fig. 7. The relationship between the TOF of methanol formation and the relative amount of m-ZrO_2 phase. Reaction conditions: $H_2/CO_2 = 3$, $T_R = 493$ K, $P = 3.0$ MPa, GHSV = 3600 h^{-1}.

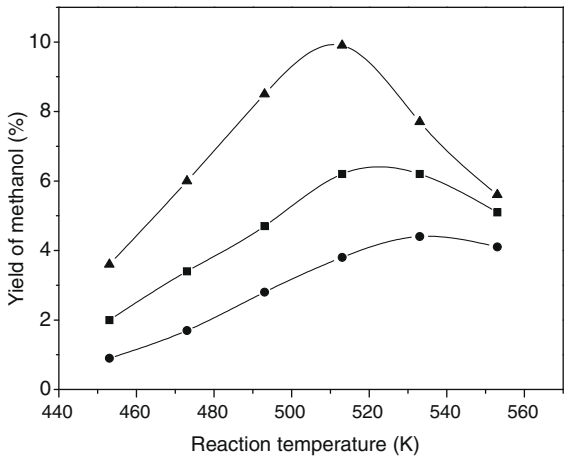

Fig. 9. Effect of reaction temperature on the yield of methanol over CuO–ZnO–ZrO_2 catalysts: (▲) 50-CZZ; (●) 100-CZZ; (■) 150-CZZ. Reaction conditions: $H_2/CO_2 = 3$, $P = 3.0$ MPa, GHSV = 3600 h^{-1}.

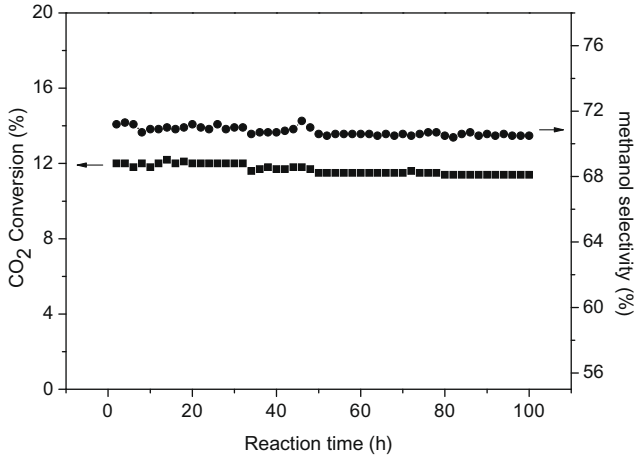

Fig. 10. Variation of CO_2 conversion and methanol selectivity with reaction time over 50-CZZ catalyst. Reaction conditions: $H_2/CO_2 = 3$, $T_R = 493$ K, $P = 3.0$ MPa, GHSV = 3600 h^{-1}.

relationship between the natural logarithm of methanol yield and the reciprocal of temperature that exists in the controlling region of kinetics, the values of apparent activation energy were calculated for methanol synthesis over different CZZ catalysts and they are 31, 40 and 34 kJ/mol for 50-CZZ, 100-CZZ and 150-CZZ, respectively. Therefore, a catalytic activity sequence of 50-CZZ > 150-CZZ > 100-CZZ is obtained, and it is in good agreement with the results aforementioned.

The stability of the most efficient 50-CZZ catalyst for CO_2 hydrogenation to methanol was measured over a 100-h period, during which the reactor was operated continuously under the test conditions. As shown in Fig. 10, the CO_2 conversion and the selectivity for methanol are found to decrease by less than 3% and 1% from its initially stabilized values, respectively. It is obvious that the CZZ sample prepared by glycine-nitrate combustion method exhibits a stable catalytic performance for the whole test period.

4. Conclusions

A series of CuO–ZnO–ZrO_2 catalysts were prepared via the glycine–nitrate combustion method with glycine from 50% to 150% of stoichiometric amount. The combustion processes and physicochemical properties of catalysts are greatly influenced by the glycine amount. The intensity of combustion and particle size of catalysts show volcano variation trends with the increase in the glycine amount, whereas opposite trends were observed for BET surface, metallic copper surface and dispersion of CuO. Meanwhile, it is found that phase transformation between *t*-ZrO_2 and *m*-ZrO_2 occurs with the changes in the glycine amount and the selectivity of methanol over *m*-ZrO_2 is higher than that over *t*-ZrO_2. The change of physicochemical properties of catalysts was related closely to the combustion intensity. The sequence of catalytic activity for methanol synthesis from CO_2 hydrogenation is in good agreement with the results of physicochemical properties, and the 50-CZZ catalyst prepared with glycine quantity being 50% of stoichiometry exhibits the highest activity. The catalytic activity of the CZZ depends not only on the surface of metallic copper but also on the phase state of ZrO_2. The glycine-nitrate combustion method was found to be a simple, fast and effective method for the preparation of CZZ catalysts.

Acknowledgments

The authors thank Shanghai Educational Development Foundation (06SG35), Science and Technology Commission of Shanghai Municipality (08520513600) and Shanghai Municipal Education Commission (J51503) for financial support. The helpful suggestions and linguistic revision of the manuscript provided by the editor (Prof. S. Ted Oyama) and anonymous reviewers are also gratefully acknowledged.

References

[1] G.A. Olah, Catal. Lett. 93 (2004) 1.
[2] R. Raudaskoski, E. Turpeinen, R. Lenkkeri, E. Pongrácz, R.L. Keiski, Catal. Today 144 (2009) 318.
[3] F. Arena, K. Barbera, G. Italiano, G. Bonura, L. Spadaro, F. Frusteri, J. Catal. 249 (2007) 185.
[4] Y. Ma, Q. Sun, D. Wu, W.H. Fan, Y.L. Zhang, J.F. Deng, Appl. Catal. A: Gen. 171 (1998) 45.
[5] R.A. Köppel, C. Stöcker, A. Baiker, J. Catal. 179 (1998) 515.
[6] J. Wambach, A. Baiker, A. Wokaun, Phys. Chem. Chem. Phys. 1 (1999) 5071.
[7] Y. Nitta, T. Fujimatsu, Y. Okamoto, T. Imanaka, Catal. Lett. 17 (1993) 157.
[8] J. Słoczyński, R. Grabowski, A. Kozłowska, P. Olszewski, J. Stoch, J. Skrzypek, M. Lachowska, Appl. Catal. A: Gen. 278 (2004) 11.
[9] J. Słoczyński, R. Grabowski, A. Kozłowska, P. Olszewski, M. Lachowska, J. Skrzypek, J. Stoch, Appl. Catal. A: Gen. 249 (2003) 129.
[10] J. Słoczyński, R. Grabowski, P. Olszewski, A. Kozłowska, J. Stoch, M. Lachowska, J. Skrzypek, Appl. Catal. A: Gen. 310 (2006) 127.
[11] F. Arena, G. Italiano, K. Barbera, S. Bordiga, G. Bonura, L. Spadaro, F. Frusteri, Appl. Catal. A: Gen. 350 (2008) 16.
[12] F. Arena, G. Italiano, K. Barbera, G. Bonura, L. Spadaro, F. Frusteri, Catal. Today 143 (2009) 80.
[13] F. Arena, L. Spadaro, O. Di Blasi, G. Bonura, F. Frusteri, Stud. Surf. Sci. Catal. 147 (2004) 385–390.
[14] R. Raudaskoski, M.V. Niemelä, R.L. Keiski, Top. Catal. 45 (2007) 57.
[15] X.M. Liu, G.Q. Lu, Z.F. Yan, J. Beltramini, Ind. Eng. Chem. Res. 42 (2003) 6518.
[16] Z.S. Hong, Y. Cao, J.F. Deng, K.N. Fan, Catal. Lett. 82 (2002) 37.
[17] Y. Choi, K. Futagami, T. Fujitani, J. Nakamura, Appl. Catal. A: Gen. 208 (2001) 163.
[18] C.L. Carnes, K.J. Klabunde, J. Mol. Catal. A: Chem. 194 (2003) 227.
[19] L.C. Wang, Y.M. Liu, M. Chen, Y. Cao, H.Y. He, G.S. Wu, W.L. Dai, K.N. Fan, J. Catal. 246 (2007) 193.
[20] G. Avgouropoulos, T. Ioannided, Appl. Catal. A: Gen. 244 (2003) 155.
[21] K.C. Patil, S.T. Aruna, T. Mimani, Curr. Opin. Solid State Mater. Sci. 6 (2002) 507.
[22] Q.G. Wang, R.R. Peng, C.R. Xia, W. Zhu, H.T. Wang, Ceram. Int. 34 (2008) 1773.
[23] Z.L. Zhang, Y.X. Zhang, Z.G. Mu, P.F. Yu, X.Z. Ni, S.L. Wang, L.S. Zheng, Appl. Catal. B: Environ. 76 (2007) 335.
[24] N.F.P. Ribeiro, M.M.V.M. Souza, M. Schmal, J. Power Sources 179 (2008) 329.
[25] M.C. Greca, C. Moraes, A.M. Segadaes, Appl. Catal. A: Gen. 216 (2001) 267.
[26] G. Avgouropoulos, T. Ioannides, H. Matralis, Appl. Catal. B: Environ. 56 (2005) 87.
[27] J.C. Toniolo, M.D. Lima, A.S. Takimi, C.P. Bergmann, Mater. Res. Bull. 40 (2005) 561.
[28] R.D. Purohit, B.P. Sharma, K.T. Pillai, A.K. Tyagi, Mater. Res. Bull. 36 (2001) 2711.
[29] D.A. Fumo, M.R. Morelli, A.M. Segadaes, Mater. Res. Bull. 31 (1996) 1243.
[30] G.C. Chinchen, C.M. Hay, H.D. Vandervell, K.C. Waugh, J. Catal. 103 (1987) 79.
[31] M.J. de Andrade, M.D. Lima, R. Bonadiman, C.P. Bergmann, Mater. Res. Bull. 41 (2006) 2070.
[32] S.R. Jain, K.C. Adiga, V.R. Pai Verneker, Combust. Flame 40 (1981) 71.
[33] J.A. Dean (Ed.), Lange's Handbook of Chemistry, 13th ed., McGraw-Hill, New York, 1985. pp. 9–14, pp. 9–19, pp. 9–25, pp. 9–66, pp. 9–67, pp. 9–82.
[34] Z.Q. Tian, H.T. Yu, Z.L. Wang, Mater. Chem. Phys. 106 (2007) 126.
[35] S. Schuyten, P. Dinka, A.S. Mukasyan, E. Wolf, Catal. Lett. 121 (2008) 189.
[36] F.A. Andrade de Jesus, R.S. Silva, A.C. Hernandes, Z.S. Macedo, J. Eur. Ceram. Soc. 29 (2009) 125.
[37] F. Deganello, G. Marcì, G. Deganello, J. Eur. Ceram. Soc. 29 (2009) 439.
[38] J.R. Zhang, L. Gao, Mater. Lett. 58 (2004) 2730.
[39] K.A. Singh, L.C. Pathak, S.K. Roy, Ceram. Int. 33 (2007) 1463.
[40] L.C. Wang, Q. Liu, M. Chen, Y.M. Liu, Y. Cao, H.Y. He, K.N. Fan, J. Phys. Chem. C. 111 (2007) 16549.
[41] Y.P. Zhang, J.H. Fei, Y.M. Yu, X.M. Zheng, Energy Convers. Manage. 47 (2006) 3360.
[42] I. Melián-Cabrera, M. López Granados, J.L.G. Fierro, J. Catal. 210 (2002) 273.
[43] M.D. Rhodes, A.T. Bell, J. Catal. 233 (2005) 198.
[44] X.M. Guo, D.S. Mao, S. Wang, G.S. Wu, G.Z. Lu, Catal. Commun. 10 (2009) 1661.
[45] Q. Sun, Y.L. Zhang, H.Y. Chen, J.F. Deng, D. Wu, S.Y. Chen, J. Catal. 167 (1997) 92.
[46] M. Boudart, Chem. Rev. 95 (1995) 661.
[47] K.P. Sun, W.W. Lu, F.Y. Qiu, S.W. Liu, X.L. Xu, Appl. Catal. A: Gen. 252 (2003) 243.
[48] J. Yoshihara, C.T. Campbell, J. Catal. 161 (1996) 776.
[49] J. Toyir, P.R. de la Piscina, J.L.G. Fierro, N. Homs, Appl. Catal. B: Environ. 29 (2001) 207.
[50] T. Inui, H. Hara, T. Takeguchi, J.B. Kim, Catal. Today 36 (1997) 25.
[51] S. Fujita, S. Moribe, Y. Kanamori, M. Kakudate, N. Takezawa, Appl. Catal. A: Gen. 207 (2001) 121.
[52] C.V. Ovesen, B.S. Clausen, J. Schiøtz, P. Stoltze, H. Topsøe, J.K. Nørskov, J. Catal. 168 (1997) 133.
[53] K.T. Jung, A.T. Bell, Catal. Lett. 80 (2002) 63.
[54] M.D. Rhodes, A.T. Bell, J. Catal. 233 (2005) 210.